IEEE Access
Multidisciplinary | Rapid Review | Open Access Journal

Received 17 June 2022, accepted 29 June 2022, date of publication 5 July 2022, date of current version 14 July 2022.

*Digital Object Identifier 10.1109/ACCESS.2022.3188673*

RESEARCH ARTICLE

# Design Aspects and Thermal Characteristics of Single-Sided Linear Induction Motor for Electromagnetic Launch Application

**LOVESH B. XAXA[1], ADITYA KUMAR[1], R. K. SRIVASTAVA[1], (Senior Member, IEEE), R. K. SAKET[1], (Senior Member, IEEE), AND BASEEM KHAN[2], (Senior Member, IEEE)**

[1]Department of Electrical Engineering, Indian Institute of Technology (BHU), Varanasi, Varanasi, Uttar Pradesh 221005, India
[2]Department of Electrical and Computer Engineering, Hawassa University, Hawassa 1530, Ethiopia

Corresponding authors: R. K. Srivastava (rksrivastava.eee@iitbhu.ac.in), R. K. Saket (rksaket.eee@iitbhu.ac.in), and Baseem Khan (baseem.khan04@gmail.com)

**ABSTRACT** This paper presents the design aspects and thermal characteristics of single-sided linear induction motor (SLIM) for Electromagnetic launchers. It is designed to accelerate a 50 kg mass through a distance of 3 meters within a minuscule time to an exit velocity of 50 m/s. A study of the motor's parametric variation based on the launching requirement has been performed. Its performance characteristics are obtained using 3D FEM and verified analytically using Parseval's method. The FEM, analytical and experimental verification of the thrust characteristics of different secondary conductive sheet materials namely, aluminum, Beryllium copper and German silver shows that, the latter exhibits superior characteristics than the former two, because its thrust-velocity curve is close to inverse linear relationship (stable region of operation of LIM) , which significantly reduces the accelerating time during the launch. The designed SLIM is assessed for its thermal performance with materials having temperature-dependent electrical properties by carrying out a coupled-field FEM simulation. The conclusions demonstrate that the electromagnetic and thermal assessments are in tandem with each other as required for launching.

**INDEX TERMS** Electromagnetic launcher, SLIM, Fourier transform model, coupled-field FEM.

## I. INTRODUCTION

The existing launching methods have reached a saturation point where they cannot meet modern launcher requirements such as higher projectile velocity and specific thrust. Comparatively, the launcher costs and simplification of the equipment drastically improves with linear electromagnetic (EM) launcher, which enables an object to be propelled within a minuscule time attaining a certain high velocity using EM force [1], [2]. It finds its application in national defense, traffic and aerospace owing to its advantages which include simple structure, recyclability, controllability, etc [3], [4]. It is reported to accelerate a cannonball to a very high velocity [5]. EM catapults can also be applied to propel unmanned vehicles, tactical missiles, aircrafts and fish torpedoes [6]. Electromagnetic launchers are in use for launching drones having lesser capability for self-take off.

The use of launching technologies for space exploration has been reviewed and indicates a strong correlation with defense applications and rocket launcher systems [7], [8]. By employing the principles of railgun and coilgun, higher muzzle velocity can be achieved [9]. Due to the serious limitation of burning of the tracks as a result of arcing at the sliding contacts of such systems, several other topologies, including the tubular type induction launcher, were investigated, whose maximum speed is limited by current-collection problems [10].

While EM Gun technology is employed for low mass projectiles, EM launch of heavy mass systems rely on machines like LIM operating at comparatively lower velocity for safe launching of mass. Linear permanent-magnet machines have also gained popularity for EM launch as

The associate editor coordinating the review of this manuscript and approving it for publication was Qinfen Lu.

they overcome the low efficiency problem present in linear induction motors (LIMs), and have been successfully developed for vertical launch and EM aircraft launch (EMAL) applications [11], [12]. Once considered insurmountable, the technical barriers have yielded to focused theoretical, computational, and experimental research [13] and several countries all over the world have taken up the challenge of developing and understanding the art and science of EM launch and launchers [14]–[17].

Long-primary single-sided LIMs (SLIMs) offer higher force density and acceleration due to its secondary conductive sheet (mover) being lightweight as compared to other types of LIMs which is suited for EM launch application. Also, there is no requirement of sliding contacts for current collection. Aditionally, when combined with high temperature superconducting magnetic levitation system, long-primary SLIM would operate without any friction loss and guidance control system [18].

The current work focuses on designing an SLIM to accelerate a mass to an exit velocity and travel a distance within a short time. A mathematical model of the EM launch system (EMLS) is developed in section II. Section IV pertains to the designing of SLIM based on a study of its parametric variation. Its performance is predicted using 3D FEM MAXWELL Software and validated analytically by Parseval's method for constant current drive [22] given in the Appendix. Section V demonstrates, how the temperature distribution of the motor is also determined with materials having temperature-dependent electrical properties by carrying out a coupled-field simulation. The results are compared with those obtained by an analytical model in section VI. The designed SLIM satisfies the performance specifications. Finally, in section VII, the key challenges involved and their possible solutions are also highlighted by the authors.

A fair comparison of the proposed work is being made with few select published works in literature involving the electromagnetic as well as thermal assessment of EMLS in Table 1.

## II. MATHEMATICAL MODEL

For simplifying the modeling of the EMLS, consider a body of mass $m$ placed on a plane inclined at an angle $\theta$ with the horizontal Earth's surface. The electromagnetic force $F$ (thrust) generated by the SLIM along the inclined plane is continuously applied to the body (mover secondary of the SLIM and the payload attached to it) and it moves with a velocity $v$.

Then the equation of motion becomes,

$$F - m\frac{dv}{dt} = m\,g\,sin\theta + \mu\,(m\,g\,cos\theta - F_p) + b\,v^2 \qquad (1)$$

where $\mu$ is the coefficient of kinetic friction, $b$ is the coefficient of drag force and $F_p$ is the normal direction electromagnetic force generated by the SLIM. It will become evident in section III B from Fig. 14b, that the normal force generated by the designed SLIM is repulsive in the region

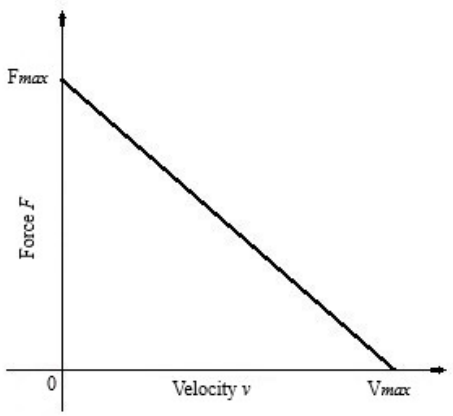


**FIGURE 1.** Assumed inverse linear force-velocity characteristic of the LIM.

of interest i.e. between standstill and a little beyond 50 m/s (exit velocity of the projectile). The secondary mover of the SLIM is considered to be placed above the primary stator. The generated normal force will levitate the mover which is controlled by friction to overcome the normal and lateral displacements. In EM launch applications, tremendous amount of electrical energy flows in the stator coils of the LIM for a short duration to provide maximum acceleration to the projectile. To avoid insulation breakdown in the coils due to the heat generated in them, the operating time of the launcher should be kept as low as possible, while achieving the desired performance. For this purpose, the characteristic between the applied force, which would be generated by the LIM stator, and the velocity must be as close to an inverse linear relationship as possible. By avoiding the positive slope region in the usual force-velocity characteristic of an LIM, the starting (accelerating) time of the motor reduces significantly. Another option is to provide a constant thrust by V/F method for launch application wherein the thrust requirement is almost half the value of peak thrust requirement in inverse linear characteristics. Though inverse linear characteristic results in quick launch. Thus, the following relation between the force F and the velocity v is assumed:

$$F = F_{max} - \frac{F_{max}}{v_{max}}v \qquad (2)$$

where $F_{max}$ *and* $v_{max}$ are the maximum limit of force and velocity starting from 0 (Fig. 1).

Equations (1) and (2) describe the accelerated motion of the body up the inclined plane. These two equations were setup in MATLAB Simulink (Fig. 2). Also, a script was written in MATLAB to find the required value of starting force $F_{max}$ to satisfy the launcher requirements.

## III. SIMULATION AND RESULTS

The following parameters (Table 2) were set for the simulation model with an aim to accelerate a body of mass 50 kg at rest to attain a velocity of 50 m/s while traveling a distance of 3 meters. With the above objective, the required

**TABLE 1. Comparison of the proposed work with published references.**

| Reference | Type of machine | EMLS | Electromagnetic Thrust Assessment | | | Thermal Assessment | | |
|---|---|---|---|---|---|---|---|---|
| | | | Analytic | FEM | Experimental | Analytic | FEM | Experimental |
| Superconducting Technology [19] | SCLSM | Civil | Multilayer theory (MLT) | Iterative | ✗ | Modeling of AC losses | Iterative | ✗ |
| Different pole Arcs [20] | PMLSM | Defence | ✗ | ✓ | ✗ | Transient heat conduction | Primary core only | Only Winding temperature |
| Different m/c topologies [21] | LIM and PMLSM | Civil | Equivalent circuit model + (MLT) | Iterative | ✗ | ✗ | ✓ + FDM | ✗ |
| Proposed work | LIM | Defence | Parseval's | ✓ | Partial | Lumped parameter mode for complete machine | Coupled EM/Mech. | Proposed for future work |

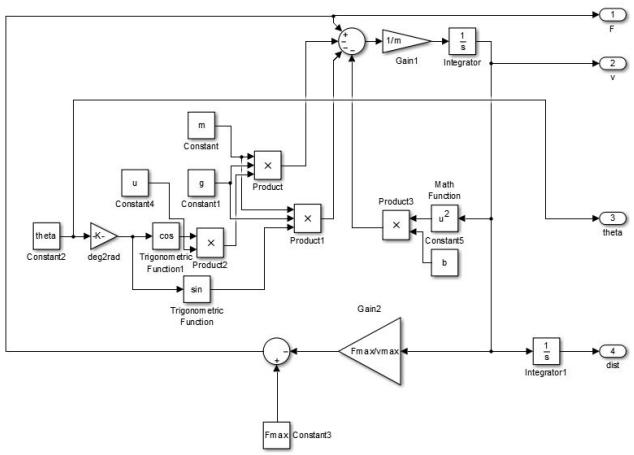


**FIGURE 2. Simulation model used for predicting SLIM performance while operating.**

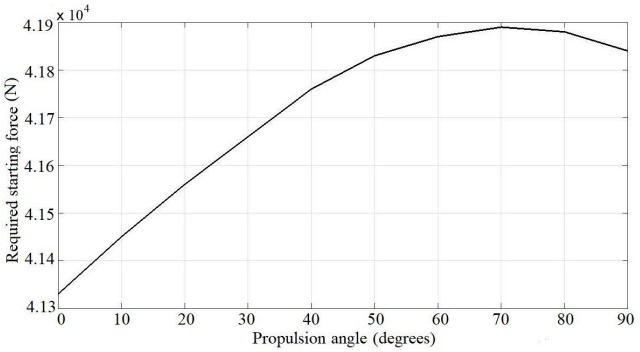


**FIGURE 3. Required values of starting force for different values of launch angle.**

values of $F_{max}$ for different values of $\theta$ were found which would satisfy the performance requirements.

Fig. 3 shows that horizontal launch of the projectile would require the least but still a considerable amount of starting force of around 41.35 kN. Also, the starting force value does not vary much (about 1.33% as compared to horizontal launch case) when the launch angle is varied. It means that the force-velocity characteristics and hence the LIM design would remain more or less the same for any launch angle between $0^o$ and $90^o$ The time to achieve the desired exit velocity can also be found, which would be crucial in deciding the operating time of the LIM and its temperature rise. Also, the power and energy required at the time of

**TABLE 2. MATLAB Simulink model parameters.**

| Parameter | Symbol | Value | Unit |
|---|---|---|---|
| Total mass of body | $m$ | 50 | kg |
| Acceleration due to gravity | $g$ | 9.81 | m/s$^2$ |
| Launch angle | $\theta$ | 0 - 90 | degrees |
| Coefficient of drag force | $b$ | 0.06 | N/m$^2$/s$^2$ |
| Coefficient of kinetic friction | $\mu$ | 0.35 | - |
| Maximum velocity | $v_{max}$ | 75 | m/s |

**TABLE 3. Design details of the SLIM.**

| Parameter | Value |
|---|---|
| Primary iron core length | 3000 mm |
| Primary iron core width | 1000 mm |
| Secondary aluminium sheet width | 3000 mm |
| Secondary back iron width | 1000 mm |
| Air gap | 10 mm |
| Secondary aluminium sheet thickness | 3 mm |
| Secondary back iron thickness | 6 mm |
| Slot width | 25 mm |
| Tooth width | 25 mm |
| Slot depth | 25 mm |
| Number of slots | 180 |
| Conductors per slot | 20 |
| Current 70 A (rms), | 99 A (peak) |
| Current density | $1.1879 \times 10^5$ A/m |
| Number of poles | 4 |
| Power supply frequency | 50 Hz |
| Stator winding arrangement | R,-B,Y, lap winding, double layer |

launching can be determined by using the force, velocity and time sample values. The results are shown for a launch angle of $30^o$, with the rest of the parameters as indicated in Table 2.

Fig. 4 shows the force-time and the inverse linear force-velocity characteristic. With a starting force of around 42 kN, it takes 0.101 seconds for the projectile to reach the exit velocity of 50 m/s within the stipulated travel distance of 3 meters. The synchronous or maximum velocity of the LIM is chosen as 75 m/s, but the projectile will exit the EMLS when it attains a velocity of 50 m/s (Fig. 4b). Figs. 4c and 4d show the predicted values of energy and power to be around 70 kJ and 694 kW respectively at the time of projectile exit.

Another study was done on the effect of variation of the parameters $\mu$ and $b$ on the required value of the starting force $F_{max}$. As is observed from Fig. 5, the value of $F_{max}$ does not vary significantly when the two coefficients are varied over their typical range of values.

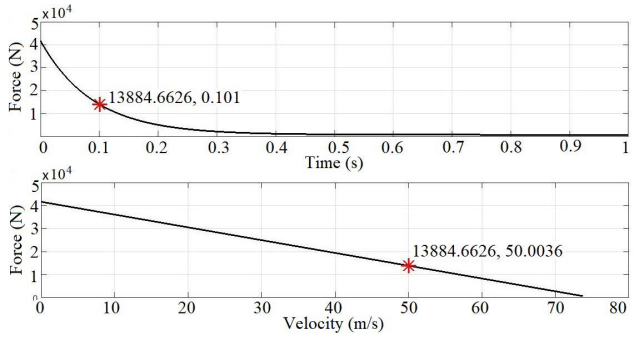


(a) Force versus time and velocity

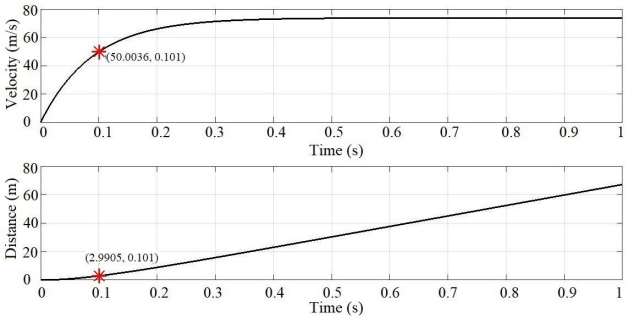


(b) Velocity and distance versus time

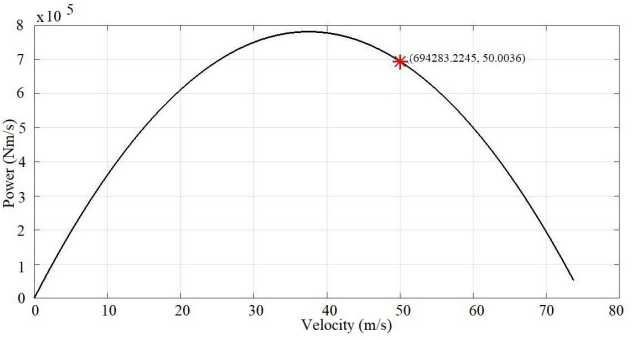


(c) Power versus velocity

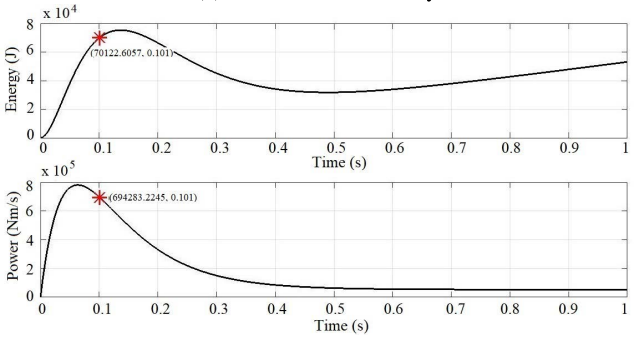


(d) Energy and Power versus time

**FIGURE 4.** Plots for a launch angle of $30^o$. The red asterisk represents the instant when the projectile exits the launcher.

## IV. DESIGN OF THE LIM

The next step is to design an LIM with a similar characteristic as obtained in Fig. 4a. Parseval's method was used to determine the force-velocity characteristics of a single-sided LIM (SLIM). It is to be noted that the length of the SLIM (stator) must be equal to the distance traveled by the projectile i.e. 3 meters

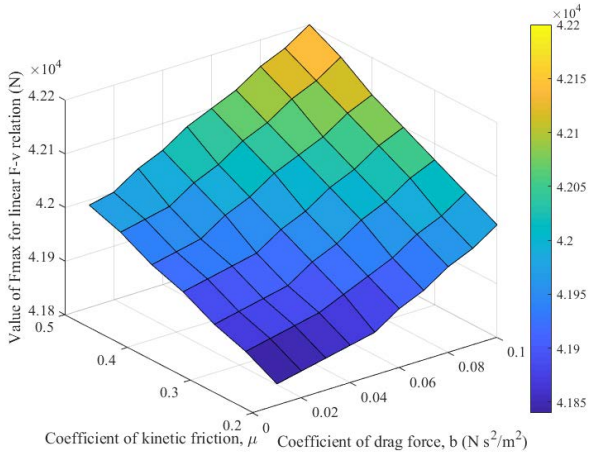


**FIGURE 5.** Surface plot of the values of the starting force $F_{max}$ for different values of coefficient of kinetic friction $\mu$ and coefficient of drag force $b$.

### A. OPTIMIZING THE DESIGN PARAMETERS

It is well known that by increasing the secondary resistance of an induction motor, linear or rotary type, its torque or force-velocity curve becomes more and more inverse linear in shape.

In order to understand the effect of varying the design parameters on the performance characteristics of the SLIM, its parametric calculation was conducted based on Parseval's method. The nominal values of the parameters, i.e the values which are kept fixed while varying a parameter, unless stated otherwise, are shown in Table 3. From the calculation results obtained for constant-current drive, Fig. 6 and 7 demonstrates the manner in which thrust alters upon varying a parameter. By increasing primary iron width (Fig. 6a), marked rise in the peak thrust can be seen. Here, the secondary conductor width is taken to be the double of primary iron width in the parametric study. It can be inferred that while decreasing the primary iron width may make the characteristic's shape more suitable for the considered application (closer to inverse-linear in shape), the thrust value would also abate. It is to be noted that the ratio of secondary and primary width is kept fixed to be 2. Fig. 6b pertains to different secondary conductor widths and again the ratio of secondary and primary width is kept fixed to be 2. The peak thrust increases almost uniformly with the increasing secondary conductor width, while the starting thrust remains very much invariable like in Fig. 6a. Fig. 6a and Fig. 6b differ on account of the Russel-Norsworthy correction factor for secondary conducting sheet resistivity being incorporated in case of the latter. The rotor resistivity increases upon decreasing the secondary conductor width. This implies higher secondary resistance, which explains the characteristics to become closer to inverse-linear in shape for smaller secondary conductor widths. Notwithstanding the above, it may be

remembered that in the case of constant voltage drive, the smaller width of primary will result in higher input current for identical input voltage and hence larger thrust. Furthermore, thrust multiplies with current square rule (Fig. 7a). Fig. 7d exhibits the behavior of the curves for different number of poles. Larger number of poles lead to greater thrust generated owing to the reduced pole pitches and thereby the synchronous velocities, for thrust falls off with increasing speed as the longitudinal (entry and exit end) effects become significant [23]. The thrust can also be made to surge by decreasing the air gap (Fig. 6d) (albeit the increase in thrust is slight when the air gap is reduced from 15 mm to 0.1 mm), supply frequency (Fig. 7c) (on account of the decrease in synchronous velocities) [24] and secondary conductive sheet thickness (Fig. 6c) (by the virtue of the reduced electromagnetic gap between the primary and the secondary iron). However, a thin layer of secondary sheet may melt and evaporate when large eddy currents will flow. As such a suitable thickness is to be selected complying Joule's limit criterion.

Fig.7b needs special inspection. Here, different metals have been evaluated for secondary sheet of conductivities in the order of $10^6$ - $10^7$ $S/m$, with the highest conductivity of aluminum at $3.77 \times 10^7$ $S/m$ and the lowest being that of German silver at $3.33 \times 10^6$ $S/m$. Within this range thrust increases with the lowering of the conductivity. Further lessening under this range would ensue a downturn in thrust as is indicated by the curve for carbon with conductivity of $2.88 \times 10^4$ $S/m$. It seems that German silver is the most suitable candidate for electromagnetic launch. The width of the secondary was decided on the basis of Russell-Norsworthy correction factor for secondary overhang for sheet rotor machines. The Russell and Norsworthy formula [25] gives a correction factor for the effective secondary surface resistivity $\rho_r'$ as

$$\rho_r' = \rho_r/(1-k) \tag{3}$$

where $k = \tanh\epsilon/[\epsilon(1+\tanh\epsilon\cdot\tanh\phi)]$, in which $\epsilon = \pi w/\tau$, $\phi = \pi\psi/\tau$, $w$ is half of the stator width, $\tau$ is the pole pitch and $\psi$ is the width of the overhang of the rotor plate beyond the edge of the stator. Fig. 8 shows the secondary surface resistivity versus secondary conductor width plots for fixed and variable primary iron widths. From the curves, it is observed that the rotor resistivity increases upon decreasing the secondary conductor width. The width of the secondary should be at least twice the width of the primary for it also decreases the transverse edge effect [26].

### B. EXPERIMENTAL RESULTS FOR THRUST

The fabricated static test rig of a smaller single sided linear induction motor (SLIM) is shown in Fig. 9. The design details are being given in Table 4. The significance of the parameters $L, w, d, a, b$ and $c$ will become evident in the Appendix. A prototype SLIM of smaller size than the proposed SLIM was fabricated and tested for different secondary conducting sheet materials to validate the performance characteristics of

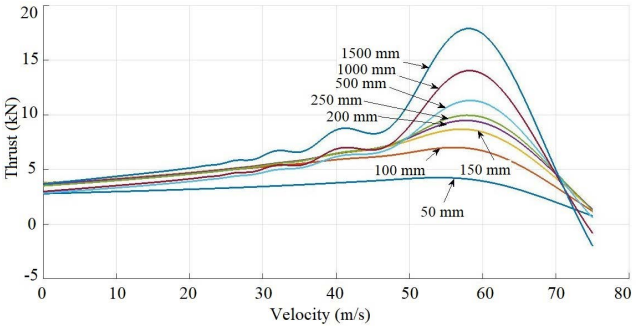


(a) Different primary iron widths

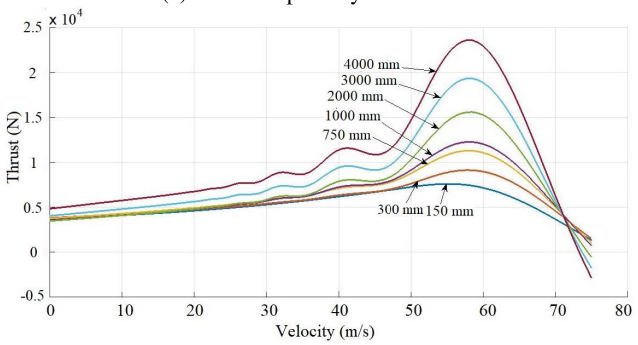


(b) Different secondary conductor widths

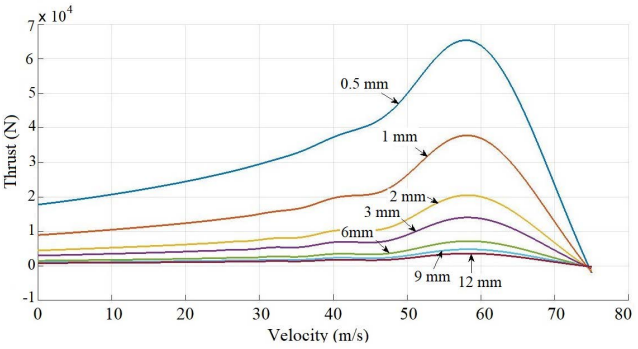


(c) Different secondary conductive sheet thicknesses

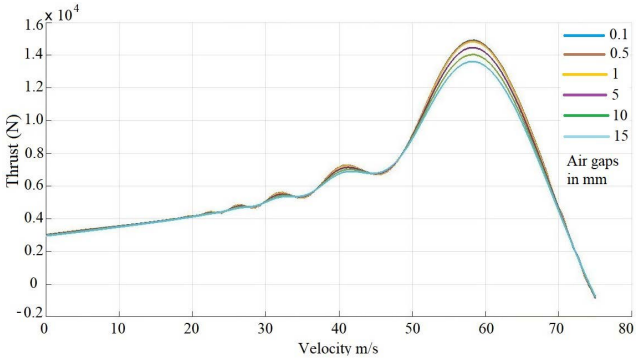


(d) Different air gaps

**FIGURE 6. Performance characteristics of SLIM with varying design parameters.**

SLIM (Fig. 7b) which is one of our conclusive suggestion in the proposed work. Fig. 10 shows the VFD inverter, DSO for ascertaining the current, the stator and the three sheet secondary plates placed in a staggered manner above the

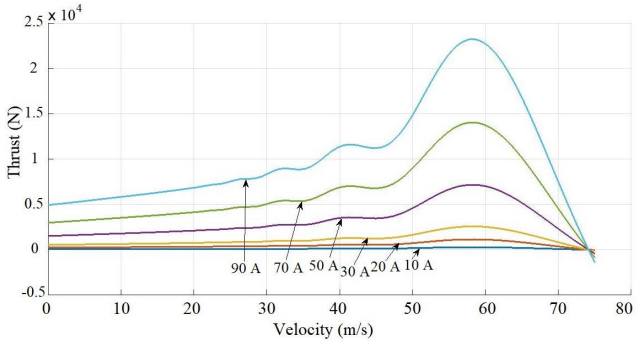


(a) Different currents

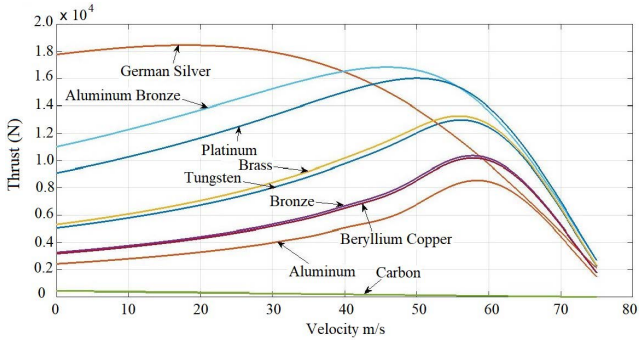


(b) Different secondary conductivities

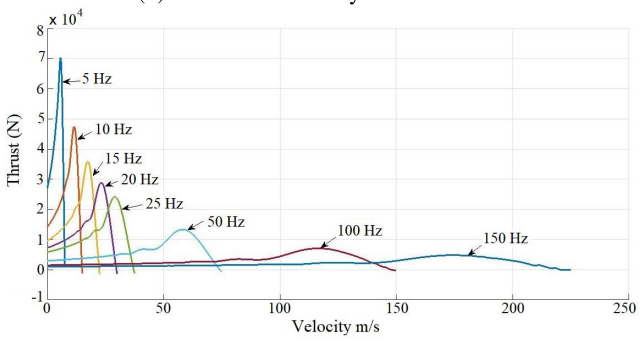


(c) Different supply frequencies

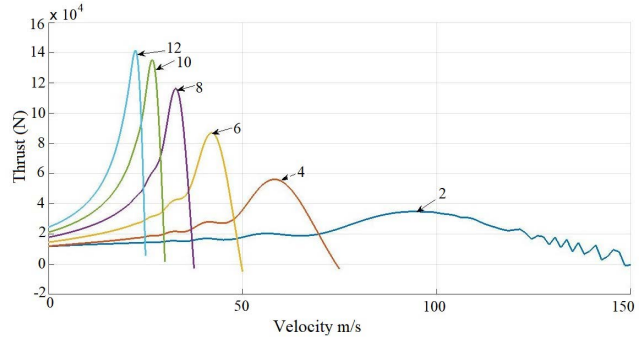


(d) Different number of poles

**FIGURE 7.** Performance characteristics of SLIM with varying design parameters [continued].

stator. The actual 3m SLIM is difficult to fabricate and test, owing to lack of finances. The sheet on the top is of aluminum with the back-iron glued above it, below of which is the sheet of German silver and the bottom sheet is of Beryllium copper. The fabricated LIMs have been theoretically analyzed

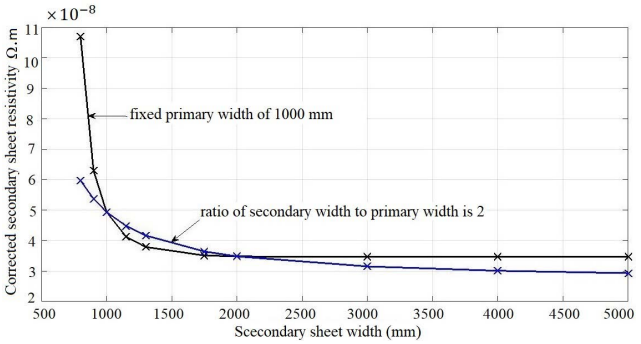


**FIGURE 8.** Effective resistivity variation due to secondary overhangs.

**TABLE 4.** Parameters of the fabricated SLIM.

| Parameter | Value |
|---|---|
| Primary iron core length ($L$, mm) | 560 |
| Secondary sheet length ($L_s$, mm) | 750 |
| Primary iron core width ($2w$, mm) | 85 |
| Secondary sheet width ($2d$, mm) | 300 |
| Secondary back iron width ($2d_i$, mm) | 145 |
| Air gap ($a - b$, mm) | 2.2 |
| Secondary sheet thickness ($b - c$, mm) | 3 |
| Secondary back iron thickness ($c$, mm) | 4 |
| Number of slots | 24 |
| Number of coils (Distributed 2 layer winding) | 30 |
| Number of coil sides per slot | 2 |
| Number of turns per coil | 50 |
| Coil pitch in terms of no. of slots | 6 |
| Pole pitch ($\tau$, mm) | 140 |
| Number of poles | 4 |
| Power supply frequency (Hz) | 50 |
| Primary Current (A) rms | 15 |

**FIGURE 9.** Prototype SLIM stator with sliding support for secondary sheet.

using Fourier transform method (Parseval's) [22] pertaining to an equivalent SLIM. The Maxwell FEM software has been used to simulate and compute fields and forces. For standstill tests, variable frequency were obtained through 18.5 kW three phase ABB make VFD (ACS-600). For linear induction motor, the Force-speed characteristics and Standstill Force versus slip frequency characteristics are quite identical with certain tolerance because of the absence of end effects in standstill condition. In the static test rig, the standstill thrust at different slip frequencies for constant current was measured using digital spring balance. The heating of the secondary plate is avoided, because it alters the conductivity of plate.

**FIGURE 10.** Setup for testing of the prototype SLIM.

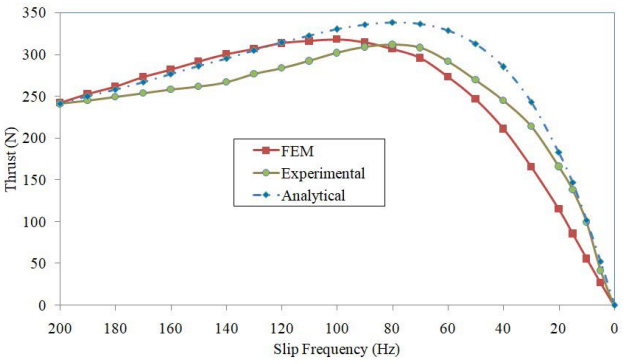


**FIGURE 11.** Thrust for SLIM with Aluminum as the secondary.

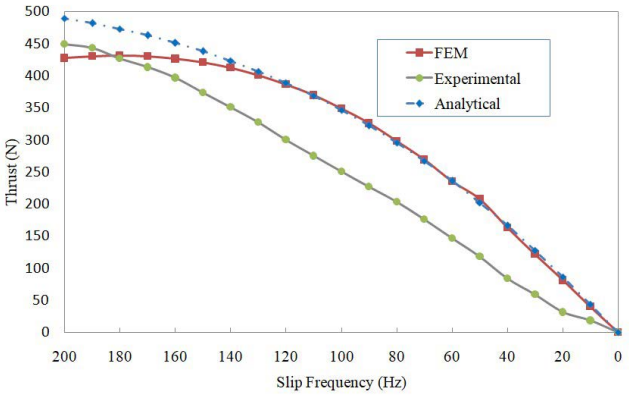


**FIGURE 12.** Thrust for SLIM with German Silver as the secondary.

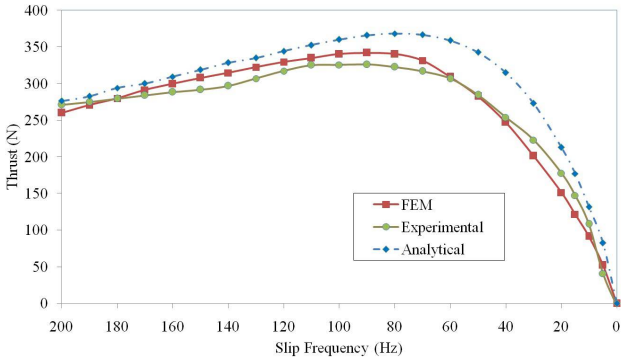


**FIGURE 13.** Thrust for SLIM with Beryllium copper as the secondary.

While Fig. 11 depicts the constant current (15A) normalized values measured and computed force of developed SLIM at different slip frequencies for aluminum as the secondary, Fig. 12 pertains to German Silver and Fig. 13 to Beryllium copper (conductivity of $2.865 \times 10^6 S/m$). The characteristics of aluminum and Beryllium copper are quite identical. All the above three materials were of non-magnetic grade. The Finite Element and analytically computed forces are on the higher side due to the assumptions made and also because of slightly unbalanced three phase supply obtained during experimentation. It can be inferred that German Silver gives better thrust characteristics than aluminum as the secondary sheet material. It also has a higher melting point than that of aluminum.

### C. SLIM DESIGN

The design parameters of the SLIM are chosen based on the study of parameter variation done and which are shown in Table 3. The above design of the SLIM is analyzed using Parseval's method and its performance characteristics are obtained (Fig. 14a and 14b). The force-velocity characteristic obtained in Fig. 14a needs to be amplified by a factor of about 4 in order to satisfy the conditions of the 3 m distance travel and 50 m/s exit velocity.

This can be done by doubling the conductors per slot, as force is proportional to current density squared. The performance of the then designed SLIM for launch application was predicted by using the developed Simulink Model. In place of the inverse-linear relation between force and velocity, the actual characteristics of the designed SLIM are used for establishing the relation between force and velocity.

Fig. 15 shows the predicted performance of the designed SLIM-assisted EMLS, which seems to be poorer than that observed for the ideal case (Fig. 4). The projectile takes about 0.143 seconds to reach the velocity of 50 m/s in 3 meter travel. The energy and power values at the time of exiting the launcher are around 256 kJ and 1.7 MW respectively, both of which are considerably higher than the values obtained for the ideal case. This goes on to show how the design of the SLIM would affect its launch performance and power supply and cooling requirements.

### D. MODEL SLIM DESIGN

A 36 cm-long model SLIM (Fig. 16) was also designed having the following parameters as detailed in Table 5.

The model SLIM was modeled and simulated in ANSYS 3D Maxwell software and its performance characteristics were obtained. The same was also verified using Parseval's method (Fig. 17).

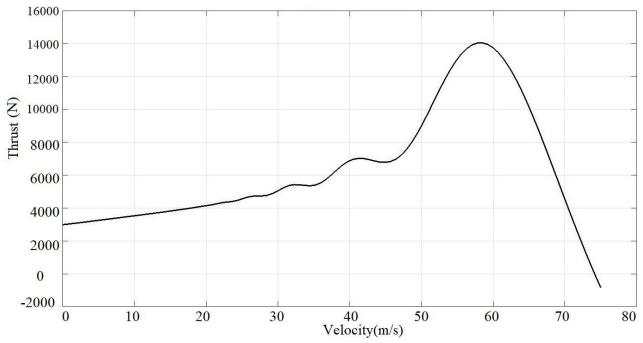


(a) Thrust-velocity characteristic

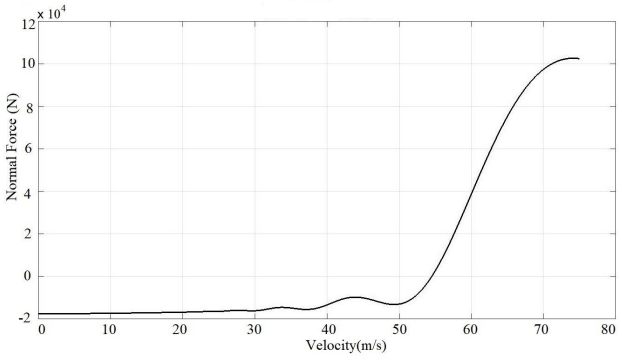


(b) Normal force versus velocity curve

**FIGURE 14.** Performance characteristics of the designed SLIM. Gain required = 3.974.

**TABLE 5.** Design details of the Model SLIM.

| Parameter | Value |
|---|---|
| Primary iron core length | 360 mm |
| Primary iron core width | 100 mm |
| Secondary aluminium sheet width | 250 mm |
| Secondary back iron width | 100 mm |
| Air gap | 15 mm |
| Secondary aluminium sheet thickness | 2 mm |
| Secondary back iron thickness | 300 mm |
| Slot width | 8 mm |
| Tooth width | 7 mm |
| Slot depth | 10 mm |
| Number of slots | 24 |
| Conductors per slot | 50 |
| Current 49.5 A (rms), | 70 A (peak) |
| Current density | $2.33 \times 10^5$ A/m |
| Number of poles | 4 |
| Power supply frequency | 50 Hz |
| Stator winding arrangement | R,-B,Y, lap winding, double layer |

## V. THERMAL CHARACTERISTICS OF THE LIM

In EM launch application, large amount of energy flows through the LIM for a short duration of time. In such condition, it becomes important to predict the thermal performance of the machine. This section describes the thermal modeling of the LIM using heat balance equation. Also, ANSYS Maxwell and Mechanical are coupled and the model is solved for temperature distribution using FEM.

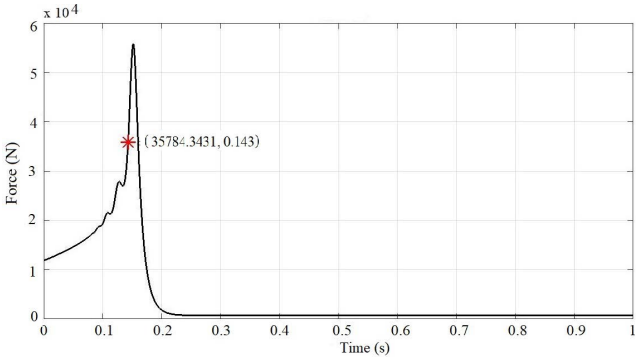


(a) Force versus time curve

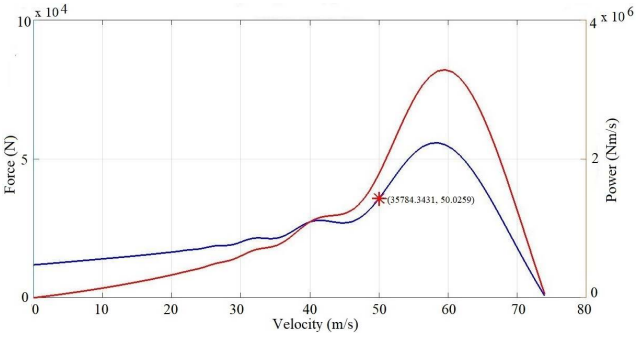


(b) Force and power versus velocity curves

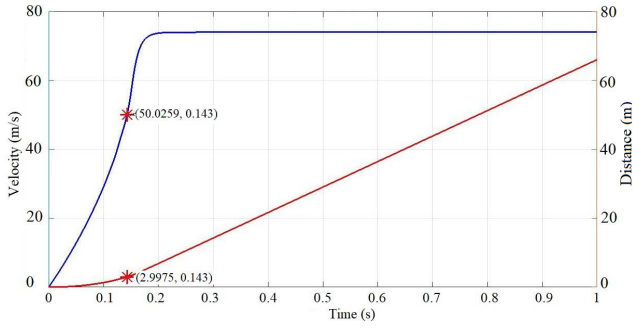


(c) Velocity and distance versus time curves

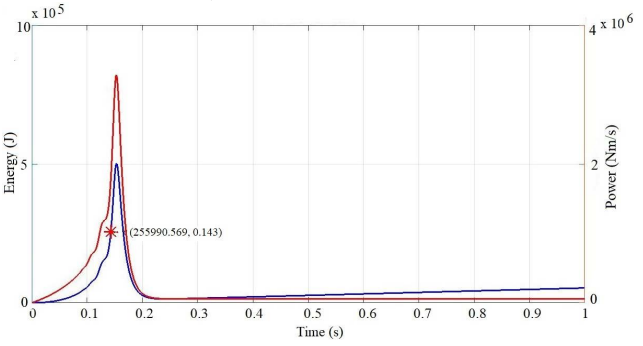


(d) Energy and power versus time curves

**FIGURE 15.** Plots for launch using the designed SLIM. The red asterisk represents the instant when the projectile exits the launcher.

### A. THERMAL MODEL

Inherently, electrical machines consist of different parts made up of different materials like copper, iron and aluminum. By following a lumped parameter approach, it is possible to estimate the temperature rise in any part of the machine, the

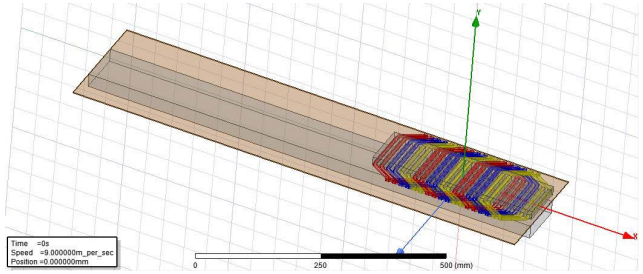

**FIGURE 16.** 3D model of the model-SLIM.

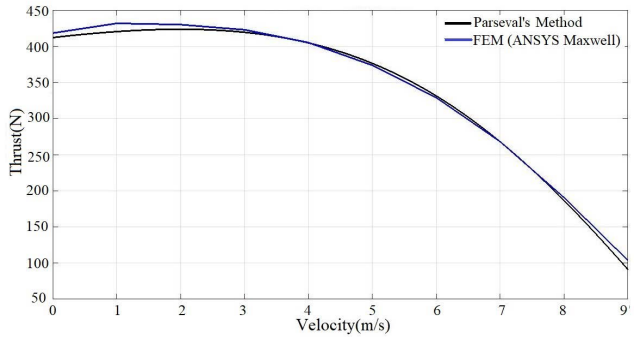


(a) Thrust-velocity characteristic

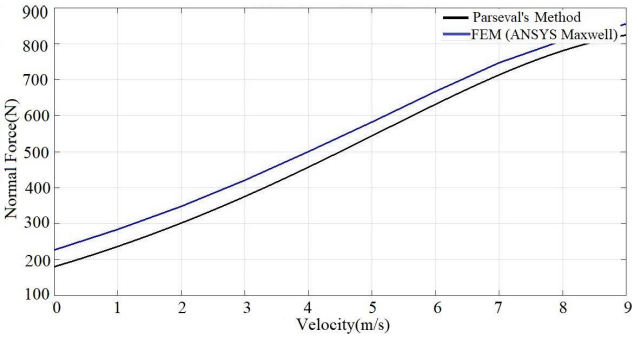


(b) Normal force-velocity characteristics

**FIGURE 17.** Performance characteristics of the model SLIM obtained by the two methods.

underlying assumption being that the temperature distribution is uniform over the surface of the body.

Let $P_1$ = heat developed, W

$P_2$ = heat dissipated to the cooling medium, W

$W$ = weight of the active part of the machine, kg $h$ = specific heat, J/kg/°C;

$A$ = cooling surface area, $m^2$

$d$ = coefficient of heat transfer, J/sec/m$^2$/°C; and

$\theta$ = mean temperature rise,°C.

During $dt$, let the machine temperature rise by $d\theta$. Then,

$$\begin{aligned} \text{Heat absorbed} &= \text{Heat developed - Heat dissipated} \\ W\ h\ d\theta &= P_1\ dt - P_2\ dt \\ W\ h\ d\theta &= P_1\ dt - \theta\ dA\ dt \\ \frac{d\theta}{dt} + \frac{D}{C}\theta &= \frac{P_1}{C} \end{aligned} \tag{4}$$

where $C = W.h$ is the thermal capacity of the machine in W/°C and $D = d.A$ is the heat dissipation constant in W/°C. Using the heat balancing Eq. (4), the temperature distribution in any part of the machine can be determined [27]. Eq. (4) can be solved for temperature rise using Laplace transform and its expression during heating is obtained as

$$\theta(t) = \theta_m(1 - e^{\frac{-t}{\tau}}) + \theta_\circ . e^{\frac{-t}{\tau}} \tag{5}$$

where $\theta_\circ$ is the initial temperature in °C, $\theta_m = P_1/D$ is the steady-state temperature rise in °C and $\tau = C/D$ is the heating time constant in $/sec$.

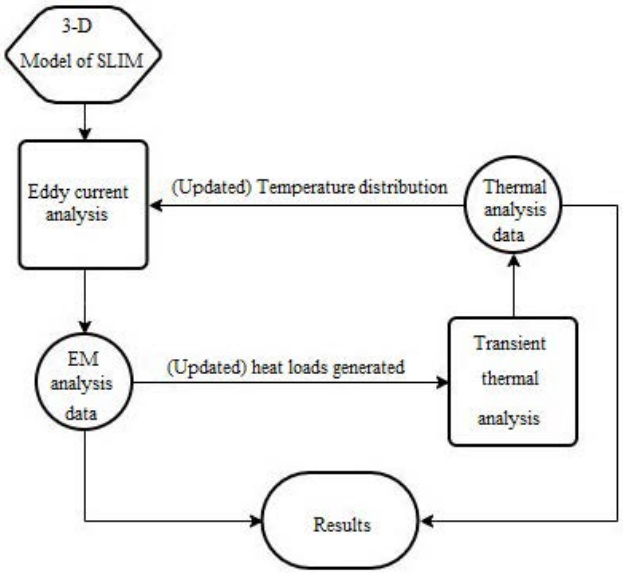


**FIGURE 18.** Flowchart of two-way coupling between ANSYS/Maxwell and Mechanical/Thermal.

### B. TWO-WAY COUPLING

In order to determine the temperature distribution in the LIM in ANSYS, the calculated losses in Maxwell are exported to ANSYS Mechanical. This coupling between these two softwares enables only one-way transfer of data. The thermal analysis data can also be fed back to the EM solver, which then updates the properties of the materials based on the imported temperature distribution and re-solves the model and generates new loss distribution. Such an analysis is called a two-way coupling and is described in Fig. 18.

Such an analysis describes the real world case where the properties of the materials such as bulk conductivity vary with temperature, resulting in non-uniform distribution of heat. The iterative process of the two-way coupling can be continued until the solution stops changing within a desired level of tolerance.

## VI. RESULTS

The designed SLIM model was solved for the temperature distribution in its coils and the aluminium sheet for standstill condition. The simulation was performed for the heat generated being applied to the bodies for 1 second, though it must be noted that the projectile exits the launcher

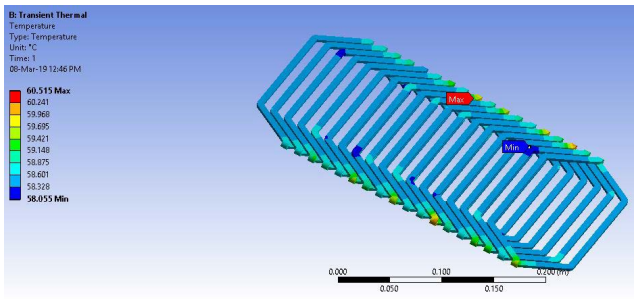


(a) Temperature distribution in the coils of the model SLIM

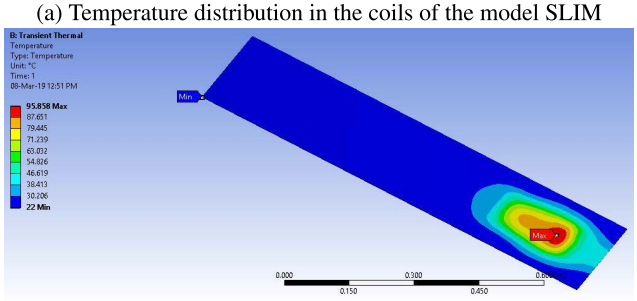


(b) Temperature distribution in the aluminum sheet of the model SLIM

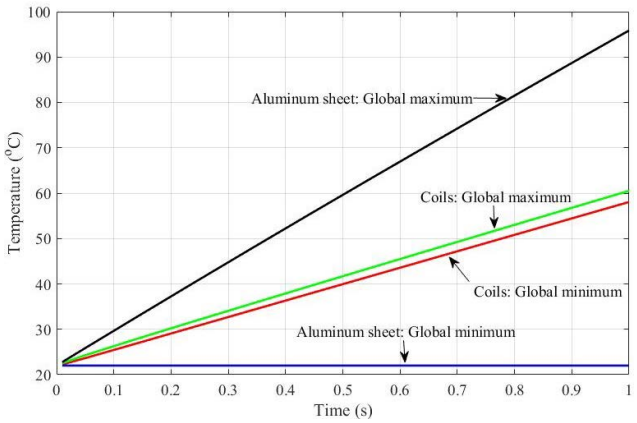


(c) Temperature of the coils and aluminum sheet of the model SLIM computed using ANSYS Workbench

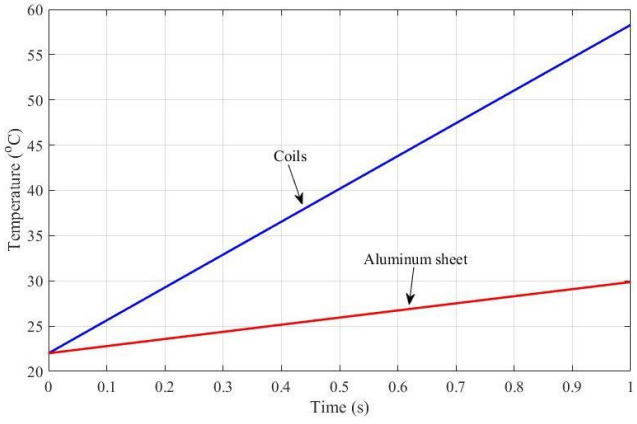


(d) Temperature of the coils and aluminum sheet of the model SLIM computed analytically

**FIGURE 19.** Results of thermal analysis of model SLIM.

within 0.15 seconds. The results obtained from the analytical thermal model and the FEM software are compared.

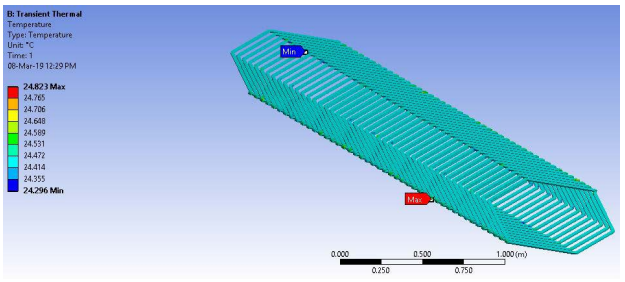


(a) Temperature distribution in the coils of the long SLIM after first iteration

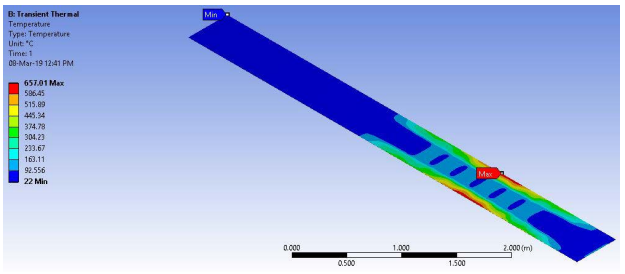


(b) Temperature distribution in the aluminum sheet of the long SLIM after first iteration

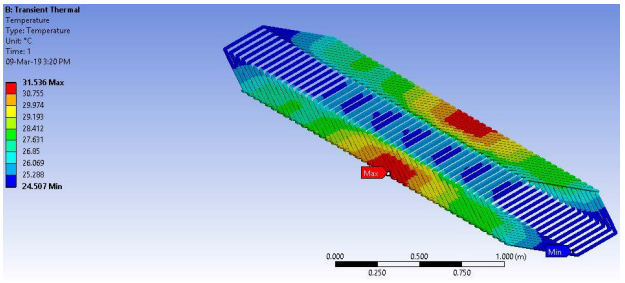


(c) Temperature distribution in the coils of the long SLIM after second iteration

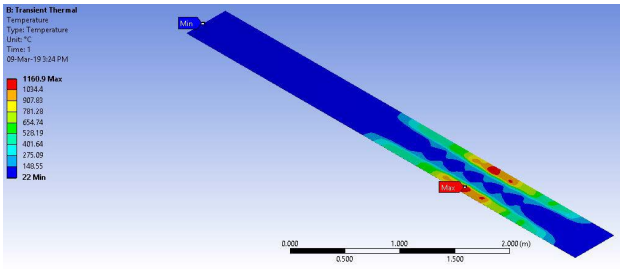


(d) Temperature distribution in the aluminum sheet of the long SLIM after second iteration

**FIGURE 20.** Results of thermal analysis of long SLIM.

### A. MODEL SLIM

Fig. 19 shows the results obtained for the designed model SLIM. In the FEM Simulation, the temperature rise in the coils is about $38°C$ (from $22°C$ to $60°C$), which is close to the value predicted by the analytical model.

However, for aluminum sheet, the distribution of temperature turns out to be very non-uniform in the simulation, the highest temperature reached being around $95°C$. The analytical model performs badly for this case and predicts the maximum temperature of the aluminum sheet to be $30^oC$ after 1 second.

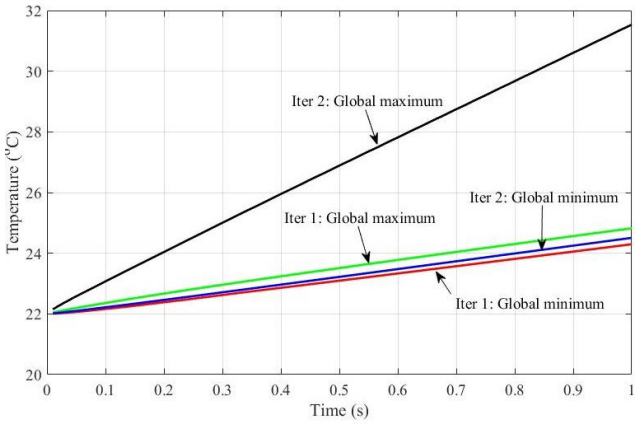


(a) Temperature of the coils of the long SLIM in the first and second iterations of two-way coupling

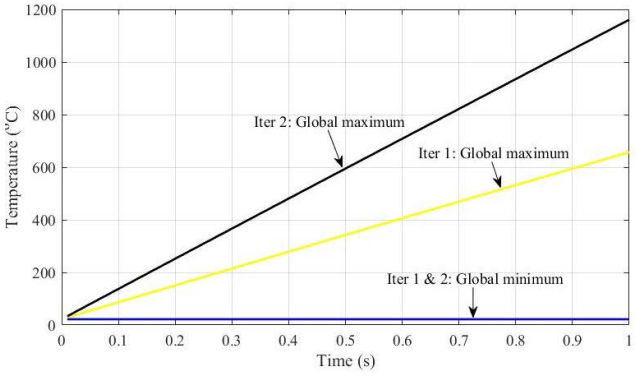


(b) Temperature of the aluminum sheet of the long SLIM in the first and second iterations of two-way coupling

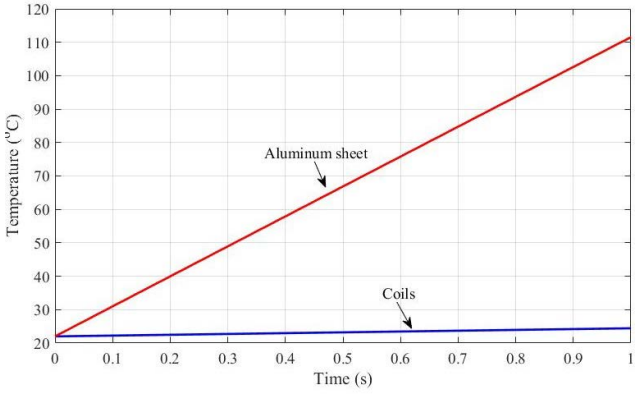


(c) Temperature of the coils and aluminum sheet of the long SLIM computed analytically

**FIGURE 21. Comparison of results of thermal analysis of long SLIM.**

### *B. LONG SLIM*

Two-way coupling between the EM and thermal solvers was employed when the long SLIM was analyzed in ANSYS Workbench. Fig. 20 shows the temperature distribution in the coils and the aluminum sheet after the first and second iteration of the simulation after 1 second. It is evident from the results that the temperature dependence of the bulk conductivities of materials such as copper and aluminum strongly affect their temperature distribution. After the first iteration, the temperature distribution is almost uniform in the coils, and hence, the analytical model predicts its temperature with high accuracy (Fig. 21).

The analytical model fails for the aluminum sheet, as was observed in the model SLIM case too. After the second iteration of the simulation, the temperature after 1 second increases for both the coils and the sheet. Moreover, the temperature distribution has become non-uniform for the coils too. It is because of this non-uniformity and the inability of the model to adapt itself with changes in conductivities that it fails to predict the temperature values with accepted level of accuracy. Another important aspect of temperature rise in the machine can be observed by comparing Fig. 19a and 20a. While the model SLIM is much shorter in length than the long SLIM, the surface area available for the coils to dissipate the heat generated in them is higher for the long SLIM. The model SLIM has a total power loss of 21.24 kW in its winding, whereas the long SLIM has that value equal to 182.44 kW (after first iteration). Still, the temperature rise is greater for the model SLIM. This observation can also be made by making the derivative term in Eq. (4) equal to zero (steady-state). Then, the steady-state temperature rise, $\theta_m = P_1/D = P_1/(d.A)$, which shows that the final steady temperature rise is directly proportional to the power loss and inversely proportional to the cooling surface area. Thus, for the same power loss, the machine having smaller dissipating surface area or poor ventilation would attain higher temperature rise.

## VII. CONCLUSION

The main conclusions and suggestions drawn on the basis of analysis, investigation and experimentation are enumerated as follows:

1) Designing an SLIM for EM launch application involves shaping its thrust-velocity curve to be inverse-linear which is in itself a challenging task. By reducing the secondary conductive sheet thickness and increasing the air clearance, the characteristic seems to become closer to what is desired but too thin of the secondary sheet might result in its melting. Also, larger air gap means more magnetizing current drawn from the supply to deliver the same power output, implying increased losses and hence temperature rise. German silver (non-magnetic grade) has been identified as the most suitable material for the secondary conductive sheet of the SLIM for EMLS because its thrust-velocity curve is close to inverse linear relationship (stable region of operation of LIM), which significantly reduces the accelerating time during the launch. Further, alternative materials such as zirconium-copper alloy can be opted for the primary winding wire and secondary conductor which have higher melting points and can withstand greater thermal stresses.
2) The analytical model for thermal simulation of LIM follows a lumped approach and fails to capture the many practicalities and non-idealities of temperature

distribution. To overcome this limitation, either this simple model can be further refined to define multiple lumps in the system or an FEM-based simulation can be conducted to accurately predict the temperature rise in the aluminum sheet, which is presented in the work.

3) The study reports constant current and frequency design of EMLS. It has been observed that constant thrust versus speed of launch for the same exit velocity yields lesser thrust requirements. However, it requires the Variable Voltage Variable Frequency (VVVF) technology for its operation and also, the launch is a bit delayed. Furthermore, the mechanical time constant of such energy machines are comparable to its electrical time constant, rendering VFD control difficult to implement.
4) The study indicates the need of either increasing the supply frequency or going for a multi-section stator, with each section having progressively increasing frequency by employing Rising Frequency Generator (RFG). A variable pole pitch LIM is also suggested with compensating windings which overcomes the design challenge.

The forthcoming advanced work is undertaken as follows:

1) These machines are subjected to very high voltage 3-phase pulse power. The presence of unstable zone (positive slope) in the transient thrust-speed characteristics, oscillations in thrust may occur during the launch. The analysis of the transient current and dynamic thrust to assess the stability of the launch is being undertaken.
2) The experimental assessment of Thermal aspects of this research work is proposed for the future work by envisaging heat sensors to be employed for recording the surface temperatures of the stator and coils of the prototype SLIM.
3) In the present work, double layer, full pitch winding has been assumed. Several other winding configurations are also envisaged like single layer winding and tooth (polar) windings for obtaining optimum operation.

Further studies involve the EMI/EMC aspects of such machines.

## APPENDIX
## PARSEVAL's METHOD OF FOURIER TRANSFORM APPLICABLE FOR LINEAR INDUCTION MOTOR

The following symbols are defined for the different parameters of the SLIM as shown in Fig. 22:
$L$: Primary stator length
$w$: Half width of Primary iron (stator core)
$d$: Half width of Secondary conductor plate
$a-b$: Air gap
$b-c$: Thickness of secondary conductive sheet
$c$: Thickness of secondary backiron
$J_m$: Primary current density
$P$: Number of poles

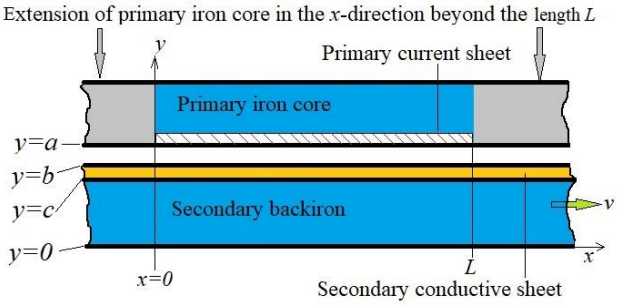


**FIGURE 22.** Model of single-sided linear induction motor [22].

$\tau$: Pole pitch
$\sigma_1$: Conductivity of iron
$\sigma_2$: Conductivity of secondary conductive material
$\mu_0$: Permeability of air
$\mu_1$: Permeability of iron
$\mu_2$: Permeability of secondary conductive material
$n$: order of harmonic representing transverse variation of field by means of Fourier series
$\xi$: The Fourier space Transform counterpart of x-coordinate, or wave number in per meters

Then, the thrust of the SLIM is given by:

$$F_t = \frac{\mu_3 J_m^2}{\pi}\int_{-\infty}^{\infty}\frac{1-cos(\xi+k)L}{\xi(\xi+k)^2} \cdot\sum_n c_n\frac{\eta_n}{\lambda_n}\Im\left[\frac{W_n(\xi,a)}{K_n(\xi)}\right]\sin\lambda_n w\, d\xi \tag{6}$$

where,

$$J_m = \frac{\sqrt{2}\times \text{Slots}\times \text{Cond. per slot}\times \text{Current}}{L} \tag{7}$$

$$k = \frac{\pi}{\tau}\quad \textit{Wave constant, per meter} \tag{8}$$

$$\lambda_n = \frac{n\pi}{2d},\ n = 1,3,5\ldots \tag{9}$$

$$c_n = \frac{2\sin\lambda_n w}{\lambda_n d} \tag{10}$$

$$\eta_n = \sqrt{\xi^2+\lambda_n^2} \tag{11}$$

$$\chi_n = \sqrt{\xi^2+\lambda_n^2+j\omega\mu_1\sigma_1+j\xi v\mu_1\sigma_1} \tag{12}$$

$$\gamma_n = \sqrt{\xi^2+\lambda_n^2+j\omega\mu_2\sigma_2+j\xi v\mu_2\sigma_2} \tag{13}$$

$\lambda_n$ is the index number of the Fourier series in the transverse direction

$c_n$ is the coefficient of the Fourier series expansion of the rectangle, which represents the primary current in the transverse direction

$\eta_n$, $\chi_n$ and $\gamma_n$ are the Fourier layer indices of air, backiron and secondary sheet respectively.

$$K_n(\xi) = \cosh\eta_n(a-b)\cosh\gamma_n(b-c)\left\{1+\frac{\mu_0}{\mu_1}\frac{\chi_n}{\eta_n}\tanh\chi_n c\right\} + \sinh\eta_n(a-b)\cosh\gamma_n(b-c)\left\{1+\frac{\mu_1}{\mu_0}\frac{\eta_n}{\chi_n}\tanh\chi_n c\right\}$$

$$+\cosh\eta_n(a-b)\sinh\gamma_n(b-c)\times\left\{\frac{\mu_0}{\mu_2}\frac{\gamma_n}{\eta_n}+\frac{\mu_1}{\mu_2}\frac{\gamma_n}{\chi_n}\tanh\chi_n c\right\}+\sinh\eta_n(a-b)\sinh\gamma_n(b-c)\times\left\{\frac{\mu_2}{\mu_0}\frac{\eta_n}{\gamma_n}+\frac{\mu_2}{\mu_1}\frac{\chi_n}{\gamma_n}\tanh\chi_n c\right\} \quad (14)$$

$$W_n(\xi,y)=\cosh\eta_n(y-b)\cosh\gamma_n(b-c)\cdot\left\{1+\frac{\mu_1}{\mu_0}\frac{\eta_n}{\chi_n}\tanh\chi_n c\right\}+\sinh\eta_n(y-b)\cosh\gamma_n(b-c)\left\{1+\frac{\mu_0}{\mu_1}\frac{\chi_n}{\eta_n}\tanh\chi_n c\right\}+\cosh\eta_n(y-b)\sinh\gamma_n(b-c)\times\left\{\frac{\mu_2}{\mu_0}\frac{\eta_n}{\gamma_n}+\frac{\mu_2}{\mu_1}\frac{\chi_n}{\gamma_n}\tanh\chi_n c\right\}+\sinh\eta_n(y-b)\sinh\gamma_n(b-c)\times\left\{\frac{\mu_0}{\mu_2}\frac{\gamma_n}{\eta_n}+\frac{\mu_1}{\mu_2}\frac{\gamma_n}{\chi_n}\tanh\chi_n c\right\} \quad (15)$$

Also, the total attracting force is given by:

$$F_p=F_{px}+F_{py}+F_{pz} \quad (16)$$

where,

$$F_{px}=-\frac{\mu_0 J_m^2 d}{4\pi}\sum_{n=1}^{\infty}c_n^2\int_{-\infty}^{\infty}\frac{1-\cos\xi L}{(\xi+k)^2}\,d\xi \quad (17)$$

$$F_{py}=\frac{\mu_0 J_m^2 d}{4\pi}\int_{-\infty}^{\infty}\sum_{n=1}^{\infty}c_n^2\left[\frac{1-\cos\xi L}{\xi^2(\xi+k)^2}\eta_n^2\left|\frac{W_n(\xi,y)}{K_n(\xi)}\right|^2+\frac{1-\cos\xi L}{\xi^2}\frac{\lambda_n^2}{k^2}\left|\frac{W_n(0,y)}{K_n(0)}\right|^2-\frac{\eta_n\lambda_n}{k}\frac{2(1-\cos\xi L)}{\xi^2(\xi+k)}\Im\left\{\frac{W_n(\xi,y)}{K_n(\xi)}\frac{W_n(0,y)}{K_n(0)}\right\}\right]d\xi \quad (18)$$

$$F_{pz}=-\frac{\mu_0 J_m^2 d}{4\pi}\sum_{n=1}^{\infty}\lambda_n^2 c_n^2\int_{-\infty}^{\infty}\left(\frac{1-\cos\xi L}{\xi^2(\xi+k)^2}\right)\cdot\left(+\frac{1-\cos\xi L}{\xi^2 k^2}+\frac{2(1-\cos\xi L)}{k\xi^2(\xi+k)}\right)d\xi \quad (19)$$

The method of performing the numerical integration can be found in [28].

## ACKNOWLEDGMENT

The authors are thankful to the Department of Electrical Engineering, IIT (BHU), Varanasi, for providing the necessary structural aid.

## REFERENCES

[1] H. Wu, B. Kou, and L. Li, "The research of a novel brushless DC linear motor for electromagnetic launcher," in *Proc. 14th Symp. Electromagn. Launch Technol.*, Jun. 2008, pp. 1–4.
[2] Q. Li, G. Chen, L. Xu, Z. Lin, and L. Zhou, "An improved model for effectiveness evaluation of missile electromagnetic launch system," *IEEE Access*, vol. 8, pp. 156615–156633, 2020.
[3] K. Baoquan, L. Liyi, and Z. Chengming, "Analysis and optimization of thrust characteristics of tubular linear electromagnetic launcher for space-use," *IEEE Trans. Magn.*, vol. 45, no. 1, pp. 250–255, Jan. 2009.
[4] I. Eguren, G. Almandoz, A. Egea, G. Ugalde, and A. J. Escalada, "Linear machines for long stroke applications—A review," *IEEE Access*, vol. 8, pp. 3960–3979, 2020.
[5] A. Egeland, "Birkeland's electromagnetic gun: A historical review," *IEEE Trans. Plasma Sci.*, vol. 17, no. 2, pp. 73–82, Apr. 1989.
[6] L. Liyi, H. Yusheng, and L. Xiaopeng, "Research of novel electromagnetic catapults with many kinds of uses," *IEEE Trans. Magn.*, vol. 41, no. 1, pp. 474–477, Jan. 2005.
[7] M. R. Palmer, "Synergism in research and development between electromagnetic guns and spacecraft electric propulsion," *IEEE Trans. Magn.*, vol. 29, no. 1, pp. 706–710, Jan. 1993.
[8] K. Dai, Y. Yang, Q. Yin, and H. Zhang, "Theoretical model and analysis on the locally concentrated current and heat during electromagnetic propulsion," *IEEE Access*, vol. 7, pp. 164856–164866, 2019.
[9] J. M. Schroeder, J. H. Gully, and M. D. Driga, "Electromagnetic launchers for space applications," *IEEE Trans. Magn.*, vol. 25, no. 1, pp. 504–507, Jan. 1989.
[10] E. R. Laithwaite, "Induction coil guns for hypervelocities," *IEE Proc. - Electr. Power Appl.*, vol. 142, pp. 215–221, May 1995.
[11] N. S. Lobo, H. S. Lim, and R. Krishnan, "Comparison of linear switched reluctance machines for vertical propulsion application: Analysis, design, and experimental correlation," *IEEE Trans. Ind. Appl.*, vol. 44, no. 4, pp. 1134–1142, Jul. 2008.
[12] D. Patterson, A. Monti, C. W. Brice, R. A. Dougal, R. O. Pettus, S. Dhulipala, D. C. Kovuri, and T. Bertoncelli, "Design and simulation of a permanent-magnet electromagnetic aircraft launcher," *IEEE Trans. Ind. Appl.*, vol. 41, no. 2, pp. 566–575, Mar. 2005.
[13] H. D. Fair, "The science and technology of electric launch," *IEEE Trans. Magn.*, vol. 37, no. 1, pp. 25–32, Jan. 2001.
[14] R. Alimi, A. Borenstein, C. Goldenberg, L. Perelmutter, A. Pokryvailo, N. Shafir, S. Wald, E. Weiss, D. Zoler, and M. Shapira, "ETC research at Soreq NRC, Israel," *IEEE Trans. Magn.*, vol. 37, no. 1, pp. 11–15, Jan. 2001.
[15] J. W. Jung, J. S. Kim, K. H. Chung, and H. Yun, "Overview of ETC program in Korea," *IEEE Trans. Magn.*, vol. 35, no. 1, pp. 23–24, Jan. 1999.
[16] P. G. Rutberg, V. A. Kolikov, and G. A. Shetsov, "Problems, results and prospects of electric launch in Russia," *IEEE Trans. Magn.*, vol. 37, no. 1, pp. 42–45, Jan. 2001.
[17] Y. Wang, S. Cheng, and P. Zheng, "Widely developing electric launch technology in China," *IEEE Trans. Magn.*, vol. 39, no. 1, pp. 39–41, Jan. 2003.
[18] L. Zheng, J. Jin, Y. Guo, and J. Zhu, "Design and characteristics analysis of long-primary single-sided linear induction motor," in *Proc. Int. Conf. Appl. Supercond. Electromagn. Devices*, Sep. 2009, pp. 85–88.
[19] L. Bertola, T. Cox, P. Wheeler, S. Garvey, and H. Morvan, "Superconducting electromagnetic launch system for civil aircraft," *IEEE Trans. Appl. Supercond.*, vol. 26, no. 8, pp. 1–11, Dec. 2016.
[20] K. B. Quan, H. X. Zhen, W. Hong-Xing, and L. Li-Yi, "Thrust and thermal characteristics of electromagnetic launcher based on permanent magnet linear synchronous motors," *IEEE Trans. Magn.*, vol. 45, no. 1, pp. 358–362, Jan. 2009.
[21] L. Bertola, T. Cox, P. Wheeler, S. Garvey, and H. Morvan, "Thermal design of linear induction and synchronous motors for electromagnetic launch of civil aircraft," *IEEE Trans. Plasma Sci.*, vol. 45, no. 7, pp. 1146–1153, Jul. 2017.
[22] S. Yamamura, *Theory of Linear Induction Motors*, 2nd ed. Tokyo, Japan: Univ. of Tokyo Press, 1979.
[23] W. Xu, G. Sun, G. Wen, Z. Wu, and P. K. Chu, "Equivalent circuit derivation and performance analysis of a single-sided linear induction motor based on the winding function theory," *IEEE Trans. Veh. Technol.*, vol. 61, no. 4, pp. 1515–1525, May 2012.
[24] G. Lv, D. Zeng, and T. Zhou, "An advanced equivalent circuit model for linear induction motors," *IEEE Trans. Ind. Electron.*, vol. 65, no. 9, pp. 7495–7503, Sep. 2018.
[25] Q. Lu, Y. Li, Y. Ye, and Z. Q. Zhu, "Investigation of forces in linear induction motor under different slip frequency for low-speed maglev application," *IEEE Trans. Energy Convers.*, vol. 28, no. 1, pp. 145–153, Mar. 2013.

[26] Q. Lu, L. Li, J. Zhan, X. Huang, and J. Cai, "Design optimization and performance investigation of novel linear induction motors with two kinds of secondaries," *IEEE Trans. Ind. Appl.*, vol. 55, no. 6, pp. 5830–5842, Nov. 2019.
[27] A. Sawhney, *A Course in Electrical Machine Design*, 6th ed. New Delhi, India: Dhanpat Rai & Co., 2006.
[28] R. K. Srivastava, "Characteristic of double gap SLIM under constant current excitation," *Comput. Electr. Eng.*, vol. 29, no. 2, pp. 317–325, Mar. 2003.

**LOVESH B. XAXA** received the B.E. degree in electrical engineering from the Samrat Ashok Technological Institute, Vidisha, Madhya Pradesh, India, in 2005, and the M.Tech. degree in power systems from the Indian Institute of Technology (Banaras Hindu University), Varanasi, Uttar Pradesh, India, in 2011, where he is currently pursuing the Ph.D. degree. Previously, he was a Faculty Member at the University Institute of Technology, Rajiv Gandhi University of Technology, Bhopal, Madhya Pradesh. His current research interests include design of linear induction motors, electromagnetic analysis of rotary, and linear electric machines.

**ADITYA KUMAR** received the B.Tech. degree (Hons.) in electrical and electronics engineering from the National Institute of Technology Calicut, Kerala, India, in 2017, and the M.Tech. degree (Hons.) in electrical machines and drives from the Indian Institute of Technology, Banaras Hindu University (BHU), Varanasi, Uttar Pradesh, India, in 2019. He is currently working with the Research Team of Professor R. K. Srivastava with the Department of Electrical Engineering, Indian Institute of Technology, BHU. His research interest includes linear and rotary induction motors.

**R. K. SRIVASTAVA** (Senior Member, IEEE) received the B.Tech. degree in electrical engineering, the M.Tech. degree in electrical machines and drives, and the Ph.D. degree in electrical machines from the Erstwhile Institute of Technology, Banaras Hindu University (BHU), Varanasi, India, in 1983, 1985, and 2000, respectively. He is currently working as a Professor in electrical machines and drives. He has published several research articles in international/national journals and conference proceedings. He has authored two books. His specializations are the electromagnetic field applied to electrical machines, linear induction machines, special purpose electrical machines, permanent magnets motors and generators, and eddy current brake. He was a Convener at the International Conference IEEE Uttar Pradesh Section: International Conference on Electrical, Computer, and Electronics (UPCON-2016), IIT (BHU), Varanasi. He is an Adviser and the Founder of the IEEE Industry Applications Society Student Chapter at IIT (BHU), Varanasi.

**R. K. SAKET** (Senior Member, IEEE) is currently a Professor with the Department of Electrical Engineering, Indian Institute of Technology (Banaras Hindu University), Varanasi, Uttar Pradesh, India. Previously, he was a Faculty Member at the Government Engineering College, Rewa, Madhya Pradesh, India; the Birla Institute of Technology and Science, Pilani, Rajasthan, India; the Sam Higginbottom University of Agriculture, Technology and Sciences, Allahabad, Uttar Pradesh; and the University Institute of Technology, Rajiv Gandhi University of Technology, Bhopal, Madhya Pradesh. He has provided his industrial services to Electrical Safety Division of the M.P. Electricity Board, Government of Madhya Pradesh, Ujjain Division, Madhya Pradesh, as an Electrical Safety Engineer. He has more than 20 years of academic, industrial, and research experience. He is the author/coauthor of six national/international patents, approximately 150 scientific articles, book chapters, and research papers in indexed international journals and prestigious conference proceedings. He has supervised 12 Ph.D. research scholars and 50 M.Tech. students. He has delivered many technical talks and honored as a resource person of the power system reliability engineering. His research interests include reliability engineering, electrical machines and drives, power system reliability, reliability enhancement of industrial components and systems, and reliability aspects in renewable energy systems. He is a fellow of the Institution of Engineers (India), a member of IET (U.K.), and a Life Member of the Indian Society for Technical Education, New Delhi, India. He has received many awards, honors, and recognitions for his excellent academic and research contributions including the prestigious Gandhian Young Technological Innovation Award, in 2018, appreciated by the Hon'ble President of India at Rashtrapati Bhavan, New Delhi, the Nehru Encouragement Award, in 1988 and 1990, and awarded by the Hon'ble Chief Minister of M.P. State Government, Bhopal, and the Design Impact Award, in 2018, appreciated by Padma Vibhushan Ratan Tata, Mumbai, India. He is an Associate Editor of the *IET Renewable Power Generation* (U.K.), *IET Electrical Systems in Transportation* (U.K.), and IEEE Access (USA). He is an Editorial Board Member of the *Journal of Electrical Systems* (France) and *Engineering, Technology and Applied Science Research* (Greece).

**BASEEM KHAN** (Senior Member, IEEE) received the B.Eng. degree in electrical engineering from Rajiv Gandhi Technological University, Bhopal, India, in 2008, and the M.Tech. and D.Phil. degrees in electrical engineering from the Maulana Azad National Institute of Technology, Bhopal, in 2010 and 2014, respectively. He is currently working as a Faculty Member with Hawassa University, Ethiopia. He has published more than 125 research articles in indexed journals including IEEE Transactions, IEEE Access, *Computers and Electrical Engineering* (Elsevier), *IET Generation, Transmission and Distribution*, *IET Renewable Power Generation*, and *IET Power Electronics*. Further, he has authored and edited books with Wiley, CRC Press, and Elsevier. His research interests include power system restructuring, power system planning, smart grid technologies, meta-heuristic optimization techniques, reliability analysis of renewable energy systems, power quality analysis, and renewable energy integration.